NASA CR-
151842

NASA CR-
ERIM 130100-13-F

NASA

Final Report

OPTIMUM THERMAL INFRARED BANDS FOR MAPPING GENERAL ROCK TYPE AND TEMPERATURE FROM SPACE

QUENTIN A. HOLMES AND DANIEL R. NÜESCH
Infrared and Optics Division

SEPTEMBER 1978

Prepared for
NATIONAL AERONAUTICS AND SPACE ADMINISTRATION

Johnson Space Center
Earth Resources Program Office
Houston, Texas 77058
Contract No. NAS9-15362
Technical Monitor: Robert K. Stewart/HA

ENVIRONMENTAL
RESEARCH INSTITUTE OF MICHIGAN
FORMERLY WILLOW RUN LABORATORIES, THE UNIVERSITY OF MICHIGAN
BOX 8618 • ANN ARBOR • MICHIGAN 48107

NOTICE

Sponsorship. The work reported herein was conducted by the Environmental Research Institute of Michigan under Contract NAS9-15362 for the National Aeronautics & Space Administration, Johnson Space Center, Houston, Texas 77058. Robert K. Stewart was Technical Monitor for NASA. Contracts and grants to the Institute for the support of sponsored research are administered through the Office of Contracts Administration.

Disclaimers. This report was prepared as an account of Government sponsored work. Neither the United States, nor the National Aeronautics & Space Administration (NASA), nor any person acting on behalf of NASA:

(A) Makes any warranty expressed or implied, with respect to the accuracy, completeness, or usefulness of the information, apparatus, method, or process disclosed in this report may not infringe privately owned rights; or

(B) Assumes any liabilities with respect to the use of, or for damages resulting from the use of any information, apparatus, method, or process disclosed in this report.

As used above, "person acting on behalf of NASA" includes any employee or contractor of NASA, or employee of such contractor, to the extent that such employee or contractor of NASA or employee of such contractor prepares, disseminates, or provides access to any information pursuant to his employment or contract with NASA, or his employment with such contractor.

Availability Notice. Request for copies of this report should be referred to:

National Aeronautics & Space Administration
Scientific & Technical Information Facility
P. O. Box 33
College Park, Maryland 20740

Final Disposition. After this document has served its purpose, it may be destroyed. Please do not return it to the Environmental Research Institute of Michigan.

TECHNICAL REPORT STANDARD TITLE PAGE

1. Report No.	2. Government Accession No.	3. Recipient's Catalog No.
130100-13-F		

4. Title and Subtitle

Optimum Thermal Infrared Bands for Mapping General Rock Type and Temperature From Space

5. Report Date
September 1978

6. Performing Organization Code

7. Author(s)
Quentin A. Holmes and Daniel R. Nüesch

8. Performing Organization Report No.
130100-13-F

9. Performing Organization Name and Address
Environmental Research Institute of Michigan
Infrared & Optics Division
P. O. Box 8618
Ann Arbor, Michigan 48107

10. Work Unit No.
Task 2

11. Contract or Grant No.
NAS9-15362

12. Sponsoring Agency Name and Address
National Aeronautics & Space Administration
Johnson Space Center
Earth Resources Program Office
Houston, Texas 77058

13. Type of Report and Period Covered
Final Report
January-July 1978

14. Sponsoring Agency Code

15. Supplementary Notes

Mr. Robert K. Stewart/HA was the NASA Technical Monitor for this task.

16. Abstract

A study was carried out to determine quantitatively the number and location of spectral bands required to perform general rock-type discrimination from spaceborne imaging sensors using only thermal infrared measurements. Beginning with laboratory spectra collected under idealized conditions from relatively well characterized, homogeneous samples, a radiative transfer model was employed to transform ground exitance values into the corresponding spectral radiance at the top of the atmosphere. Taking sensor noise into account analysis of these data revealed that three 1 μm wide spectral bands would permit independent estimations of rock-type and sample temperature from a satellite infrared multispectral scanner. This study, which ignores the mixing of terrain elements within the instantaneous field of view of a satellite scanner, indicates that the location of three spectral bands at 8.1-9.1 μm, 9.5-10.5 μm and 11.0-12.0 μm, and the employment of appropriate preprocessing to minimize atmospheric effects makes it possible to predict general rock-type and temperature for a variety of atmospheric states and temperatures.

17. Key Words	18. Distribution Statement
Thermal Infrared Imaging System General Geologic Mapping Multispectral Thermal Scanner	Initial distribution is indicated at the end of this document.

19. Security Classif. (of this report)	20. Security Classif. (of this page)	21. No. of Pages	22. Price
Unclassified	Unclassified	ix + 48	

PREFACE

This final report describes efforts on Task 2 which sought to determine quantitatively the optimum number and location of spectral bands required to do general rock-type discrimination using thermal IR measurements only. This study was performed within the Infrared and Optics Division of the Environmental Research Institute of Michigan under NASA Contract NAS9-15362 during the period from January - July 1978. Mr. Robert K. Stewart of the Earth Resources Program Office at the Lyndon B. Johnson Space Center, Houston, Texas was Technical Monitor for this work.

The work performed under this task represents an effort in which special emphasis should be given to a channel selection while taking into account sensor noise, atmospheric absorption as well as the available technology for satellite imaging systems in the 1982-83 time frame. This study would have fallen short of the intended goal without the significant contribution of Dr. Robert K. Vincent of Geospectra Corporation. Unfortunately, the small number of rock samples on which later thermal infrared spectral measurements and a quantitative mineral analysis had been performed limited this study technically.

This task was conducted under the guidance of Mr. Richard R. Legault, Head of the Infrared & Optics Division. Dr. Quentin A. Holmes was the Project Manager for this study. The authors wish to acknowledge the substantial contributions made to this work by Robert Horvath and Lester Witter of ERIM.

CONTENTS

FIGURES

TABLES

1
EXECUTIVE SUMMARY

Thermal infrared scanners with multiple spectral bands in the 8-14 μm wavelength region will be important for geological remote sensing because this spectral region of the electromagnetic spectrum contains unique compositional information about silicate rocks and minerals. Of special interest are the emittance minima (reststrahlen bands), which occur in igneous rocks at different wavelengths depending on silicate rock types.

A detailed study was performed to determine quantitatively the number and location of spectral bands required to do general rock-type discrimination from spaceborne sensors using only thermal IR measurements. The objective of this study was to provide empirical evidence for the evaluation of a potential imaging system in the 1982-83 time frame. To maximize economic benefits for projected users the following specific parameters have been addressed: spectral bandwidths, sensor noise, atmospheric absorption/attenuation and temperature variation within a scene.

Beginning with 134 thermal infrared rock spectra in the 8-13 μm region from samples with both weathered and polished surfaces, a radiative transfer model was used to obtain corresponding spectral radiances at the top of the atmosphere for these samples under three different atmospheric conditions and five sets of random temperatures. Results of the current study indicate that both sample temperatures and mineral composition parameters (% SiO_2, V_7, and M_{16}) can be estimated using preprocessed measurements from a spaceborne imaging sensor with three 1 μm wide spectral bands. Taking sensor noise into account, bands located at 8.1-9.1, 9.5-10.5, and 11.0-12.0 μm are expected to provide imagery with a high signal/noise ratio while permitting discrimination of materials with little or no spectral structure in the thermal infrared.

Moreover, a pair of fixed linear features ($TEMI_1$ and $TEMI_2$) of these preprocessed multispectral thermal measurements exist which correlate well with only sample temperature ($r \geq 0.77$) and rock-type ($r \geq 0.72$) respectively for scenes of geological interest.

No consideration was given to the deleterious effects of vegetation cover other than to suggest a non-linear feature, MD, which would exclude such areas from analysis. Adding a fourth spectral band from 12.0-13.0 μm would complete the spectral coverage of the thermal infrared for other applications and should further improve the ability to remotely estimate sample temperatures. The small number of thermal infrared rock spectra available from samples whose mineralogical content is unequivocally known is unfortunate and should be remedied soon. However, this investigation shows that there are strong reasons to expect that Earth-orbiting multispectral thermal infrared scanners could provide important new information for geologic mapping, while simultaneously providing more accurate temperature measurements of natural terrain features.

2
INTRODUCTION

Thermal infrared imaging systems have been the subject of research for more than a decade because of the potential they hold for natural resource exploration. Remote sensing of rock-types using the thermal region depend primarily upon broad spectral exitance minima of minerals in the 8-13 μm wavelength region (Lyon, 1964). While Lyon and Patterson (Lyon, et al, 1969) showed that narrow-bandwidth ($\Delta\lambda \leq 0.1$ μm) spectroscopy can discriminate successfully between rock-types, a low signal to noise ratio would preclude the extension of this high spectral resolution technique to airborne imaging systems. To overcome this limitation, Vincent and Thomson (1971 and 1972a) used a ratio image of two 2-3 μm wide bands from an airborne thermal infrared scanner to obtain multispectral data for discriminating between rock types in a quartz sand quarry in Oklahoma and over volcanic terrain in Southern California. Watson (1975) developed a heat transfer model for one-dimensional periodic heating of a uniformly conductive ground with radiative transfer to the atmosphere. His model is useful in the interpretation of thermal infrared images of rock formations. In particular, he exercised this model to predict optimum times for data acquisition in determining thermal properties of terrain. Vincent (1975) demonstrated that a ratio of two thermal infrared channels could be related to variations in silicates, while suppressing temperature variations within the scene. More recently Kahle (1977) derived an improved heat transfer model of the earth's surface which included what Kahle terms "sensible and latent heating". However, because the emphasis was on modeling the heat transfer of the earth's surface, Kahle ignored the spectral features of surface emissivity and atmospheric emission/absorption effects on the radiation received by the remote sensor (i.e., it was assumed that brightness or radiation temperature determined remotely is equal to the surface

temperature). Most of her test area was homogeneous in terms of spectral emittance (emissivity) and she used data collected from an aircraft flying at a low altitude.

An investigation of the improvement in rock type classification obtained by incorporating a second thermal infrared band on the Landsat-D Thematic Mapper (Holmes and Nüesch, 1978) concluded that more than two infrared bands were required to distinguish between variations in general rock-type for samples with random temperatures.

Since a multiband thermal infrared imaging system could play a large role in the mapping of rock types from space in the 1980s, it is important to determine the number and locations of spectral bands necessary to discriminate between rock-types successfully in the presence of a variety of sample temperatures, and representative effects of the earth's atmosphere and sensor noise. The major objective of this investigation was to theoretically determine whether rock composition could be determined through measurements of infrared radiances in the presence of sensor, atmospheric and thermal noise.

3
APPROACH

Before the question of the optimal number, best location and bandwidth of spectral bands for geological remote sensing can be addressed, two more basic questions arise: How should non-rock samples be screened out and on what basis should an evaluation be made? There is no universally accepted set of physical parameters which, being measured accurately by a thermal infrared scanner, would be unequivocally useful for general geological mapping. The procedure we adopted for relating sensor signals to types of igneous silicate rocks involved the following six steps:

- Separated silicate materials from everything else
- Used Vincent's parameters to connect Travis' rock chart names to the corresponding mineral composition
- Connected rock samples with spectral emittance (emissivity)
- Accounted for temperature of sample
- Accounted for contribution of atmospheric transmittance and path radiance assuming no reflected radiation
- Accounted for sensor noise

Having related sensor signals to rock chart names, the criterion used for selecting the number and locations of spectral bands was the resulting ability to predict rock-types and estimate sample temperature. However, samples used for this study were well characterized and homogeneous. No attempt has been made to account for the mixing of rock-types or other terrain elements (such as vegetation) within the instantaneous field of view of a satellite scanner.

3.1 SCREENING OUT MOST NON-SILICA TERRAIN ELEMENTS

Prior to applying a procedure for discriminating among rocks with different silica content it is desirable to discriminate between silicate

rocks and non-silica terrain elements. While silicate rocks exhibit broad emittance minima in the 9.0-11.0 μm wavelength region, non-rock materials such as vegetation and water have almost no variation in spectral emittance in the thermal infrared region (Leeman et al, 1971). Carbonate rocks such as limestone and dolomite have very narrow emittance minima at 11.4 μm and 14.0 μm, but otherwise exhibit few emissivity variations in the 8-14 μm spectral region (Hunt and Salisbury, 1975) making them amenable to the procedure described below. However, phosphates (Hunt and Salisbury, 1975) and sulphates (Leeman et al, 1971) do have spectral emittance minima in the 8-14 μm region and can hardly be screened out by the following procedure.

We have developed a non-linear Mineral Discriminant, MD, which permits screening out most non-silica terrain elements, except phosphates and sulphates as mentioned. MD is based upon the absence of distinct reststrahlen bands in the 9-11 μm wavelength region. Since spectral exitance is related to mineral composition, we approximated the exitance curve of each sample by a parabola fitted through three infrared band measurements in the 8-12 μm range. Initially we used bands at 8.2-9.0 μm, 9.0-9.8 μm and 10.5-11.3 μm; later we used the three spectral bands which were found to be "optimum for mapping rock type and temperature". Using wavelength in μm as the horizontal axis and spectral exitance in watts/cm^2 as the vertical axis, we found that the reciprocal of the focal length, f, of this parabola formed an effective discriminant against materials with little variation in spectral exitance. Defining our mineral discriminant, MD, by

$$MD = 1/f$$

we found that all of our silicate samples had values of MD less than 0.3, while vegetation and water samples correspond to much larger values of MD (indicating a relatively flat emittance curve or little evidence of reststrahlen bands). For sulphates with emittance minima in the 8.1-9.1 μm wavelength region and carbonates with minima in the 11-12 μm

region, MD would become negative. In addition, a discrimination against relatively silica-poor soils and sands with fine particle size such as clay rich soils seems feasible (Hunt and Vincent, 1968).

3.2 USING VINCENT'S PARAMETERS TO CONNECT ROCK CHART NAMES TO MINERAL COMPOSITION

3.2.1 PERCENT OF SILICON DIOXIDE (% SiO_2)

In the previous geological applications of thermal infrared remote sensing, researchers have sought to exploit the fact that some relationship exists between the position of the silicate emittance minima (reststrahlen bands) and % SiO_2 content which could be related to silicate rock types. Vincent and Thomson (1972b) correlated the "center of gravity" of the spectral emittance curves with the ratio of the two spectral bands used in their study and showed subsequently a slight correlation between the ratios and the SiO_2 content of the silicate rocks. The reasons for the general correlation between the location of the reststrahlen bands and the corresponding SiO_2 content of rock samples are still not fully understood, although considerable work has been done on the spectroscopy of igneous silicate rocks. Our computation of the correlation between the wavelength of the emittance minima and the percent SiO_2 for twenty-five igneous silicate rocks resulted in a correlation of only -0.57. Nevertheless we used % SiO_2 as one of our physical parameters because SiO_2 is an important constituent of igneous rocks and quantitative measurements of SiO_2 content by weight were available for 97 of the samples.

3.2.2 V_7 MINERALOGIC PARAMETER

There exists no widely accepted quantitative parameter which orders igneous silicate rocks according to traditional petrology. Beginning with the Travis rock chart (Travis, 1955) Vincent suggested an approach using linear combinations of seven minerals (Vincent, 1973). A one-dimensional parameter, V_7, was created to provide a continuously varying

parameter which can be gated (maximum and minimum values specified for the parameter) to discriminate among various igneous rock categories in Travis' rock chart. This empirically-based parameter is defined by the following equation:

$$V_7 = 1/3[100 + 2(\%\ \text{potassic feldspar}) + 1.5(\%\ \text{quartz}) + (\%\ \text{sodic plagioclase}) - (\%\ \text{calcic plagioclase} + \%\ \text{olivine} + \%\ \text{pyroxene} + \%\ \text{nepheline})] \quad (1)$$

where % means volume percent. V_7 has a maximum of 100 for a hypothetical rock composed purely of potassic feldspar and a minimum of 0 for a rock composed entirely of combinations of calcic plagioclase, olivine, pyroxene, and nepheline. It orders the silicate rocks into the groups listed in Table 1. As rock types progress from the left side of Travis' rock chart (represented by group A) to the right side (represented by group J) V_7 decreases from 100 to 0. Values of V_7 were available for 94 of our samples. The correlation between % SiO_2 and V_7 was 0.765 for these 94 samples.

3.2.3 M_{16} MINERALOGIC PARAMETER

The normative minerals which geologists have chosen to emphasize in traditional rock classifications do not have the same relative importance in terms of their effect on the infrared properties of rocks. The question arises as to what mineralogical parameter the thermal infrared tells the most about, even if it may not be well correlated with traditional rock type nomenclature? To help answer this question another approach was taken by Vincent (1973) by relating the ratio of radiances in two thermal infrared bands to a parameter consisting of a linear combination of the volume percentages of sixteen minerals contained in the rock sample. This parameter, M_{16}, was defined by regressing calculated ratios of two thermal bands for 25 representative rock samples against the volume percentages of the normative minerals they contained.

TABLE 1. LIMITS OF V_7 FOR ROCK GROUPS BASED ON TRAVIS' IGNEOUS ROCK CHART

Group	Equigranular Members	V_7 Ranges
A	Granite	100-84
B	Syenite	84-81
C	Nepheline Syenite	81-80
D	Quartz Monzonite	80-67
E	Monzonite	67-66
F	Nepheline Monzonite	66-65
G	Granodiorite	65-47
H	Quartzdiorite and Diorite	47-37
I	Gabbro, Diabase and Theralite	37-18
J	Peridotite	18-0

M_{16} is defined by the following equation:

$$M_{16} = B_o + \sum_{i=1}^{16} B_i m_i \qquad (2)$$

where B_o = a constant

B_i = coefficient for the volume percentage of the ith mineral

m_i = volume percentage of the ith normative mineral in this sample

The sixteen minerals considered are shown in Tables 2a and 2b. Although Travis' classification places greatest importance on quartz, potassic feldspar, feldspathoids, pyroxene and olivine with secondary importance on the relative amounts of sodic and calcic plagioclase, a stepwise regression indicated that the most significant eight minerals for predicting Vincent's infrared ratio were forsterite, anorthite, wollastonite, water, magnetite, hematite, albite and quartz in that order.

3.3 SPECTRAL DATA SOURCES

To obtain the best available data set we began by manually digitizing 134 rock spectra in the wavelength region from 8-13 μm. These spectral emittance measurements include 26 igneous silicate rocks with broken and weathered surfaces (Vincent, 1973), 76 igneous rocks (Hunt and Salisbury, 1974), and 32 metamorphic rocks (Hunt and Salisbury, 1976). All of the spectra we used from Hunt were taken over large (representative) surface areas of samples which had been polished (see Appendix).

TABLE 2. MINERALOGICAL INDEX M_{16}

2a: m_i represent volume percentages of the minerals below

Symbol	Mineral	Symbol	Mineral
m_1	Olivine	m_9	Apatite
m_2	Wollastonite	m_{10}	Orthopyroxene (Magnesium Rich)
m_3	Water	m_{11}	Nepheline
m_4	Hematite	m_{12}	Corundum
m_5	Albite	m_{13}	Clinopyroxene (Iron Rich)
m_6	Quartz	m_{14}	Clinopyroxene (Calcium Rich)
m_7	Olivine	m_{15}	Clinopyroxene (Magnesium Rich)
m_8	Ilmenite	m_{16}	Orthopyroxene (Iron Rich)

2b: B_o and B_i have the following values (Vincent, 1973)

B_o	= 1.360600	B_9	= 0.120840
B_1	= -0.002417	B_{10}	= 0.005732
B_2	= 0.350000	B_{11}	= -0.006352
B_3	= -0.013110	B_{12}	= 0.008251
B_4	= -0.112930	B_{13}	= 0.189930
B_5	= -0.002834	B_{14}	= -0.129250
B_6	= -0.001032	B_{15}	= 0.128740
B_7	= 0.022932	B_{16}	= -0.011553
B_8	= -0.090608		

3.4 SAMPLE TEMPERATURE

Sample temperature has a greater effect than spectral exitance on thermal infrared radiance detected by most multispectral scanners. If thermal infrared scanner data are collected only during periods when temperature variations within the scene of interest are small, estimation of sample temperature may not be necessary for mapping exitance variations across the scene. In the more likely case where there are significant temperature variations in the scene (several occurrences of the same rock type with different surface temperatures) discrimination between rock types will be more reliable if some form of correction is made on detected radiance for sample temperatures. As long as a given material doesn't undergo a change of state, the spectral emittance (emissivity) is nearly independent of temperature for most common materials and for temperature of the terrestrial environment. Therefore the spectral exitance at any given temperature and wavelength can be calculated if the emissivity,† ε, is known or vice versa (graybody assumption). However, silicate rocks as selective radiators exhibit broad spectral emittance minima in the 9-11 μm wavelength region. This variety of spectral structures, which is caused by inter-atomic vibrations (Vincent, 1975), makes it necessary to have more than one thermal infrared band to estimate, or compensate for sample temperatures. We did not assume that all the samples were at the same temperature. Instead we drew a temperature for each sample from a Gaussian temperature distribution whose mean value was 300°K and which had a standard deviation of 5°K. Moreover, to enable temperature effects to be isolated from emittance minima the drawing of 134 random temperatures was done five times to obtain a data base of 670 samples.

†Emissivity, $\varepsilon(\lambda)$, is defined as the ratio of the radiant exitance of a material to the radiant exitance of a blackbody at the same temperature.

3.5 ATMOSPHERIC TRANSMITTANCE AND PATH RADIANCE

A thermal infrared radiative transfer model (Anding et al, 1970) was used to transform each of these individual rock spectra into the corresponding spectral radiance at the top of the atmosphere. During these computations we assumed that in the thermal region solar radiation reflected by the sample is negligible. Figures 1 and 2 illustrate the spectral dependence of atmospheric transmittances and path radiances predicted by this radiative transfer model for the three atmospheres used in this study. Although ozone plays an important role in atmospheric absorption, particularly near the 9.64 μm wavelength region, water content of the atmosphere plays a more dominant role in radiative transfer through the atmosphere in the thermal infrared region. Thus, temperate winter (atmosphere b) represents the best viewing condition, the tropical atmosphere (atmosphere c) the poorest, and the arctic summer atmosphere (atmosphere a) represents an intermediate condition for thermal observations for this study.

3.6 SENSOR NOISE

Sensor signals were obtained by integrating spectral radiances at the top of the atmosphere over each spectral band. Sensor noise was simulated by quantizing the sensor signals into intervals of $\sqrt{12}$ · noise equivalent photons radiance difference (Holmes, et al, 1978). We used 3.2×10^{14} photons sec^{-1} cm^{-2} sr^{-1} as the noise equivalent photon radiance difference for each thermal band.

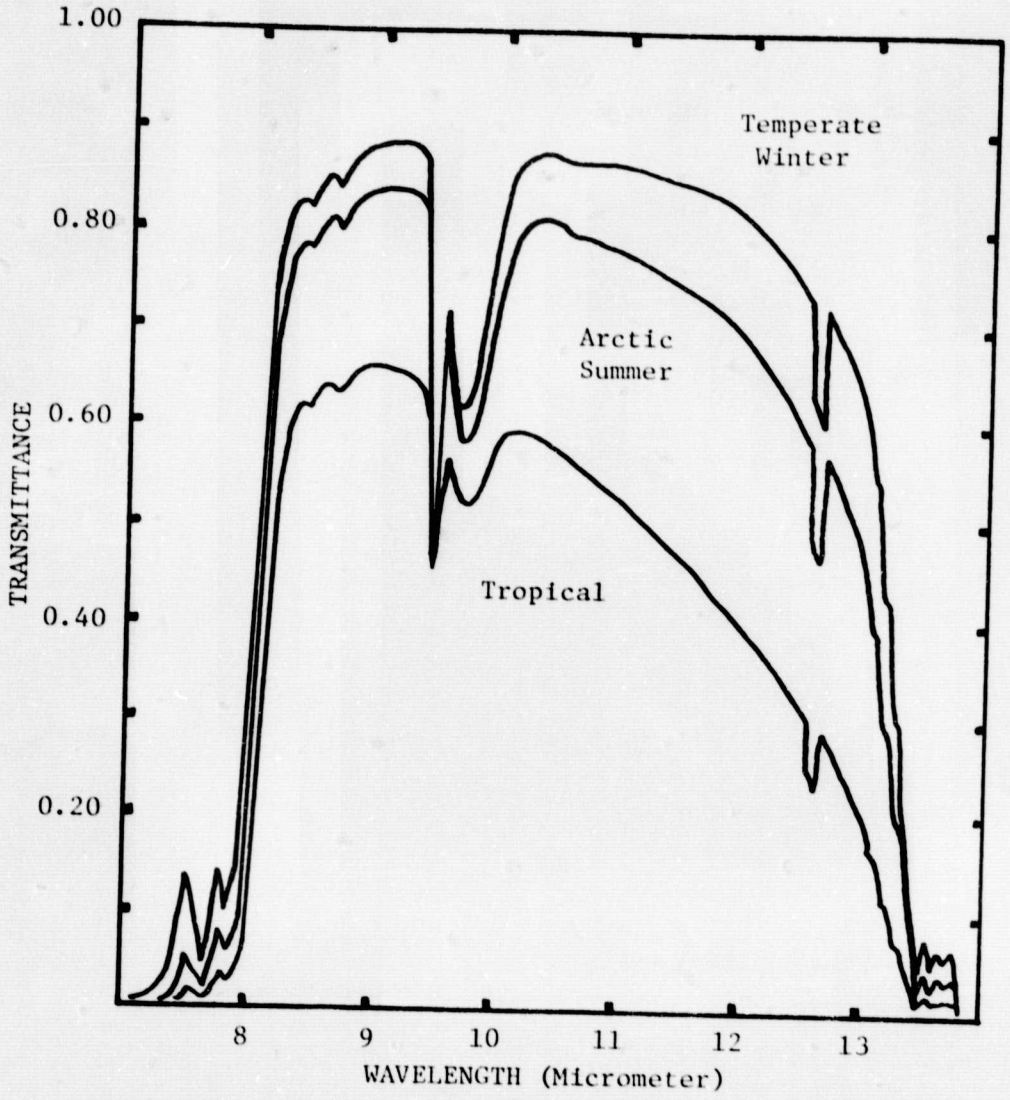

FIGURE 1. ATMOSPHERIC TRANSMITTANCE

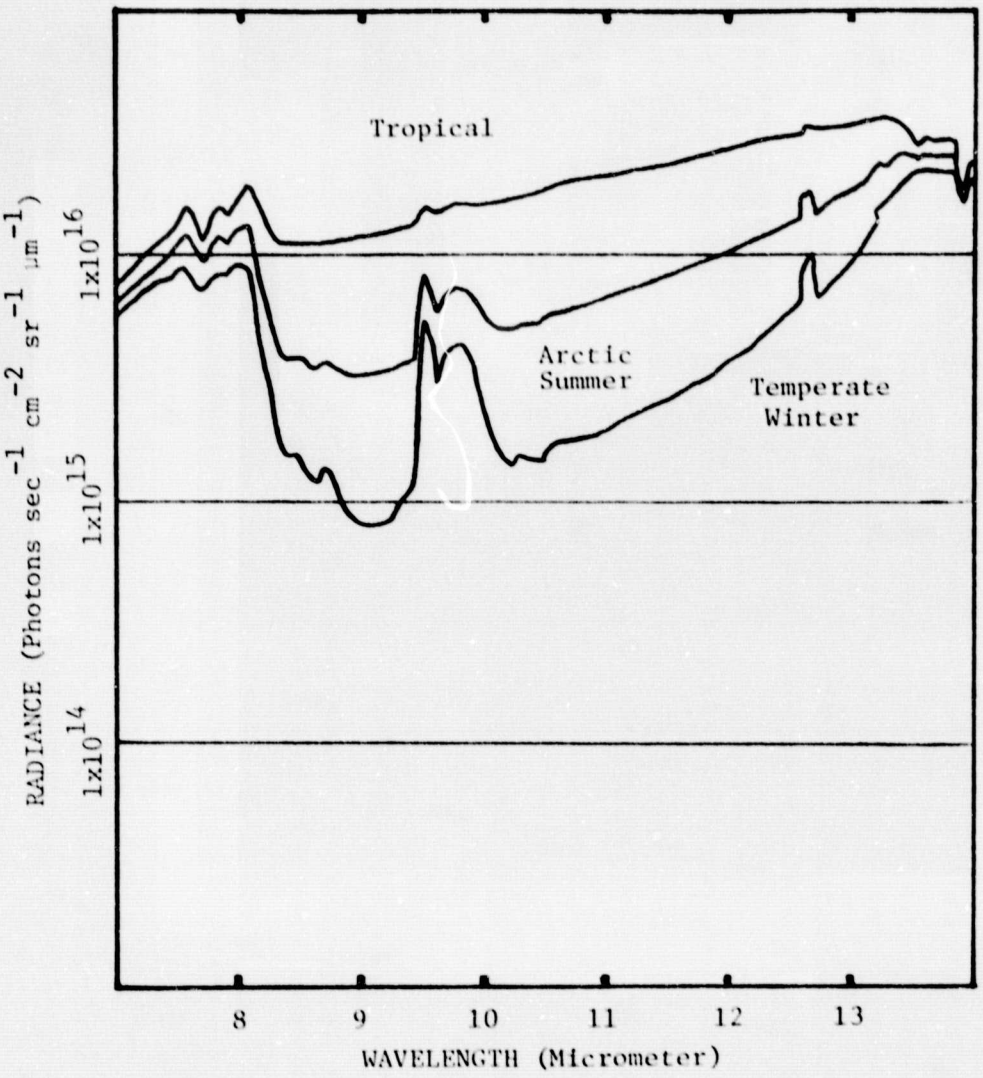

FIGURE 2. ATMOSPHERIC PATH RADIANCE

4
DETERMINATION OF THE NUMBER OF SPECTRAL BANDS

4.1 AN UPPER BOUND ON PERFORMANCE

For a given atmosphere and sample temperature, numerical integration of the spectral radiance of each sample as viewed from the top of the atmosphere over fifty 0.1 μm-wide spectral interval steps in the 8-13 μm wavelength region produced a fifty-dimensional sample vector. Such a measurement could, in theory, be made by a noise-free "fifty-channel thermal infrared scanner". In the calculation of these vectors each sample was given five different random temperatures to enable temperature effects to be isolated from compositional structure. To us these vectors represented a control, i.e., they served to indicate the "best achievable" performance when these samples are viewed through the atmosphere without regard to sensor noise or practical limitations on the number of spectral bands. A measure of this performance was obtained by linear regression of these fifty dimensional vectors for the best viewing condition to predict sample temperature, % SiO_2, and V_7 (M_{16} was only available for Vincent's samples). The resulting r^2 values were: for temperature, $r^2 = 0.943$; for % SiO_2, $r^2 = 0.739$; and for V_7, $r^2 = 0.723$. (Note: These r^2 values would <u>not</u> have been unity even if the atmosphere had not been included.) Thus our intent was to determine the number of spectral bands, hopefully not too large, above which the point of diminishing returns is reached. This viewpoint was motivated by an analogous situation in the visible region of the spectrum for Landsat (Wheeler et al, 1976).

4.2 INDEPENDENCE OF SAMPLE TEMPERATURE AND COMPOSITION

A principal component analysis on three sets (one for each of the atmospheres used in this study) of 670 sample vectors indicated that in each case the first three principal components accounted for almost all (99.90%) of the data variability. Moreover, in each case a linear

combination (hereafter called a linear feature) of the measurements could be found which was independent of sample temperature and which would correlate quite well with rock-type parameters (% SiO_2, V_7, M_{16}). Unfortunately, the coefficients of these linear features were different for each of the three atmospheric conditions used in this study.

4.3 PREPROCESSING

To overcome this limitation and to permit the use of broader spectral bands a preprocessing technique which minimized the influence of the atmosphere on the ensemble of observations was developed. The specific form of preprocessing employed is based upon the role sample emissivity and temperature play in radiative transfer through the atmosphere. Explicitly,

$$L_{ij} = \varepsilon_{ij}\, L(T_j)\, \tau_i + L_i^{Path} + 0 \text{ (reflected radiation)} \qquad (3)$$

where the index i denotes the ith spectral band and the index j denotes the jth picture element in a scene. L_{ij} is the radiance measured by the ith band of the sensor when viewing an object with emissivity ε_{ij} and temperature T_j, through an atmosphere of transmittance τ_i and path radiance L_i^{Path} (we omit any contributions from reflected radiation). Neglecting terms involving the combined effects of emissivity and temperature, subtraction of the scenic mean from each observation yields a value which is proportional to atmospheric transmission times the sum of two terms.

$$\text{i.e.,} \quad \bar{L}_i = \bar{\varepsilon}_{ij}\, L(\bar{T})\, \tau_i + L_i^{Path} \qquad (4)$$

$$\text{so,} \quad L_{ij} - \bar{L}_i = (A_i\, \Delta\varepsilon_{ij} + B_i\, \Delta T_j)\tau_i \qquad (5)$$

The first term on the right-hand side of Equation 3 is proportional to the deviation of the sample emissivity from the mean emissivity of the

scene, while the second term is proportional to the deviation of the sample temperature from the mean temperature of the scene.

Assuming that the standard deviation of the measurements in a given spectral band is proportional to atmospheric transmittance, the preprocessed measurements are

$$Y_{ij} = \frac{L_{ij} - \bar{L}_i}{(\sigma_i^2 - \sigma_n^2)^{1/2}} = A_i \Delta\varepsilon_{ij} + B_i \Delta T_j \qquad (6)$$

where Y_{ij} is defined as the preprocessed signal corresponding to the signal in the ith thermal band from sample j,

L_{ij} is the radiance in the ith thermal band from sample j,

$\bar{L}_i$ is the scenic mean for the ith thermal band,

σ_i^2 is the variance of $\bar{L}_i$ in the ith thermal band,

σ_n^2 is the variance of the signal contributed by the sensor,

$\Delta\varepsilon_{ij}$ is the deviation of the emissivity in the ith band of the jth sample from the mean emissivity of the scene in the ith band,

ΔT_j is the deviation of the temperature of the jth sample from the mean temperature of the scene,

while A_i and B_i are constants.

Since spectral exitance is related to composition, we began with the idea of approximating the emittance curve of each sample by an arbitrary choice of six 0.8 μm wide spectral bands. However, we observed that as far as temperature and % SiO_2 were concerned, three spectral bands accounted for the data variability percentages almost as well as four, five, or six spectral bands. Thus we focused our attention on three spectral bands (8.2-9.0, 9.0-9.8, 10.5-11.3 μm) and examined the

linear features of this three-dimensional data set for 25 of Vincent's samples. The first principal component was found to account for 79% of the variation in this data set. The second principal component was virtually independent of sample temperature (correlation = 0.004) yet accounted for 20% of the variation in the data set. Moreover, when the preprocessed signals (Y_i) from Hunt's samples were used in the regression developed on principal component one of Vincent's samples we were able to predict temperatures for Hunt's samples with a correlation of 0.71 and a bias of 2°K. The corresponding predictions of SiO_2 and V_7 values using the Y_is from Hunt's samples in conjunction with the second principal component from Vincent's samples gave correlations of -0.77 and -0.59 respectively. Encouraged by these preliminary results we set about determining an optimum set for the three spectral bands.

5

DETERMINATION OF THE OPTIMUM THREE SPECTRAL BANDS

To reduce the computational burden the final locations of the three thermal infrared spectral bands were arrived at in stages.

Because the intent was to determine spectral bands suitable for use from space, the atmospheric window from 8-13 μm was divided into nine 1 μm wide bands as shown in Table 3. It was felt that spectral bandwidths of this order would provide imagery with good signal/noise ratios as well as provide adequate spectral resolution for discriminating mineral composition. Among the eighty-four unique choices of nine spectral bands taken three at a time, only twenty-seven sets of three spectral bands were examined. This reduction stemmed from our observation that non-overlapping spectral bands were preferable and that it was unreasonable to locate the center of the shortest wavelength band above 9.5 μm or the center of the longest wavelength band below 10.5 μm. (The center of the reststrahlen bands usually lies in the spectral region from 9.4-10.8 μm.)

As our standard of comparison we adopted the performance of linear regressions developed on preprocessing signals from Vincent's samples (training) in predicting sample characteristics from the preprocessed signals (Y_i) computed for Hunt's samples (test). Different regressions were used for sample temperature and mineral composition.

Preprocessed signals (Y_i) for each of the nine candidate thermal bands were prepared using the best viewing conditions (atmosphere b). Sensor noise was not added at this stage. Then regressions were used to derive linear features of the Y_i to estimate sample temperature, SiO_2, V_7, and M_{16} with each of the twenty-seven sets of three spectral bands. Each three-band set was judged by how well the linear features developed on Vincent's samples (training) performed when applied to Hunt's samples (test). The three highest ranked sets were selected for more detailed analysis:

TABLE 3. CANDIDATE SPECTRAL BANDS CONSIDERED IN THE 8.0-13.0 μm WAVELENGTH REGION

Band 1	8.1- 9.1 μm
Band 2	8.5- 9.5 μm
Band 3	9.0-10.0 μm
Band 4	9.5-10.5 μm
Band 5	10.0-11.0 μm
Band 6	10.5-11.5 μm
Band 7	11.0-12.0 μm
Band 8	11.5-12.5 μm
Band 9	12.0-13.0 μm

Best prediction of % SiO_2:

Band set α: (band 1, band 4, band 7)

Best prediction of V_7:

Band set β: (band 1, band 3, band 6)

Best prediction of sample temperature:

Band set γ: (band 3, band 7, band 9)

The final stage in the determination of the best location of the three thermal infrared bands was to test the performance of spectral band sets α, β, and γ in the presence of sensor noise and variations in atmospheric viewing conditions. Sensor noise was simulated by quantizing the signal values in each spectral band. Quantized signal values for spectral configurations α, β, and γ were calculated for all 134 rock spectra using random sample temperatures to simulate variations in ground conditions. The drawing of 134 random temperatures was done five times to obtain a quantized data base of 670 samples. Three such quantized data bases were prepared -- one using atmosphere a, one using atmosphere b, and one using atmosphere c. After these quantized signals were preprocessed, linear discriminants determined for the Y_is from Vincent's samples under the best viewing conditions (atmosphere b) were used to estimate sample temperatures and mineral composition from the Y_is from first Vincent's and then Hunt's samples under all three viewing conditions.

6
RESULTS

Table 4 shows the regression results (predicted vs. true) for Vincent's samples under atmosphere b. Since the training and the test data are identical this indicates the best that one can do with three 1 μm wide thermal bands. For comparison, Table 5 shows the correlations which resulted from applying the linear discriminants developed on Vincent's samples under atmosphere b (training) to the Y_is calculated from Vincent's samples under a different atmospheric condition (test). While band set α and β retain their position in providing the best ability to predict % SiO_2 and V_7 even in the presence of sensor noise and a change in atmospheric conditions, band set γ no longer provides the best ability to predict sample temperatures. Table 6 gives the correlations resulting when these same linear discriminants are used in conjunction with the Y_is calculated from Hunt's samples under all three atmospheric conditions. Here M_{16} was excluded because it could not be determined for Hunt's samples. V_7 values for Hunt's samples were estimated by matching the sample names to categories within Travis' rock chart and then using a representative value of V_7 (e.g., Hunt's quartzdiorite was assigned a V_7 value of 45, whereas Hunt's diorite was assigned a V_7 value of 39). We note that under atmosphere c, the predictions of % SiO_2 and V_7 for Hunt's samples (last three rows of Table 6) are better than for Vincent's samples (Table 5). This is probably caused by the polished surfaces of Hunt's samples which result in more pronounced reststrahlen bands than the weathered surfaces of Vincent's samples.

Considering the results for a theoretical, noise-free "fifty-channel thermal infrared scanner" on our data set, the spectral band set α (8.1-9.1, 9.5-10.5, 11.0-12.0 μm) is seen to provide thermal infrared measurements from space with good performance for both sample temperature

TABLE 4. CORRELATION BETWEEN TRUE AND ESTIMATED VALUE OF TEMPERATURE, % SiO_2, V_7 AND M_{16} FOR VINCENT'S 25 SAMPLES UNDER ATMOSPHERE b

Band Set	Temp.	SiO_2	V_7	M_{16}
α (band 1,4,7)	0.952	0.685	0.744	0.964
β (band 1,3,6)	0.940	0.685	0.752	0.981
γ (band 3,7,9)	0.978	0.664	0.750	0.952

TABLE 5. CORRELATION BETWEEN TRUE AND ESTIMATED VALUE OF TEMPERATURE, % SiO_2, V_7 AND M_{16}. (Estimation of Vincent's 25 Samples Under Atmosphere c Based on Training Over 25 Samples Under Atmosphere b)

Band Set	Temp.	SiO_2	V_7	M_{16}
α (band 1,4,7)	0.944	0.655	0.696	0.912
β (band 1,3,6)	0.931	0.641	0.715	0.947
γ (band 3,7,9)	0.878	0.631	0.698	0.901

TABLE 6. CORRELATION BETWEEN TRUE AND ESTIMATED VALUE OF TEMPERATURE, % SiO_2 AND V_7 (Estimation of Hunt's 109 Samples Based on Training Over Vincent's 25 Samples for Atmosphere b)

	Band Set	Temp.	SiO_2	V_7
Predicting Under Atmosphere b	α (band 1,4,7)	0.774	0.729	0.773
	β (band 1,3,6)	0.747	0.711	0.593
	γ (band 3,7,9)	0.861	0.624	0.631
Predicting Under Atmosphere a	α (band 1,4,7)	0.794	0.719	0.771
	β (band 1,3,6)	0.767	0.547	0.595
	γ (band 3,7,9)	0.881	0.609	0.627
Predicting Under Atmosphere c	α (band 1,4,7)	0.769	0.670	0.740
	β (band 1,3,6)	0.747	0.651	0.580
	γ (band 3,7,9)	0.836	0.530	0.585

and mineral composition under a wide range of atmospheric conditions. We developed two fixed linear features of the preprocessed signals for spectral band set α. Feature one, which we call "$TEMI_1$", correlates excellently with sample temperature while being independent of mineral composition. Feature two, which we call "$TEMI_2$", correlates well with sample composition and is relatively insensitive to the temperature of the sample. The fixed linear features for spectral band set α were:

$$TEMI_1 = 0.52254(Y_1) + 0.56253(Y_2) + 0.64071(Y_3)$$

$$TEMI_2 = 0.74491(Y_1) + 0.06440(Y_2) - 0.66405(Y_3)$$

The correlation matrix between these features and the parameters of interest for Vincent's 25 samples is shown in Table 7.

Figures 3 through 6 show scatter plots illustrating results achieved with spectral band set α. In each instance linear regressions computed using atmosphere b were applied unchanged to samples observed under atmosphere a. A scatter plot of predicted and actual M_{16} values is shown in Figure 3. Figures 4, 5, and 6 illustrate the correlation between estimated and actual temperature, % SiO_2, and V_7 respectively for Hunt's samples. The correlation of 0.794 for temperature is excellent considering that the relationship used to predict these temperatures were developed from observation of Vincent's samples under atmosphere b.

TABLE 7. CORRELATION BETWEEN $TEMI_1/TEMI_2$ AND THE PARAMETERS TEMPERATURE, % SiO_2, V_7 AND M_{16}
(For Vincent's 25 Samples Only)

	Temp.	SiO_2	V_7	M_{16}	$TEMI_1$	$TEMI_2$
Temp.	1.0000					
SiO_2	-0.0473	1.0000				
V_7	0.0112	0.9181	1.0000			
M_{16}	0.0283	-0.7186	-0.7678	1.0000		
$TEMI_1$	0.9366	-0.0487	0.0200	-0.0808	1.0000	
$TEMI_2$	0.0655	-0.7087	-0.7565	0.9735	-0.0080	1.0000

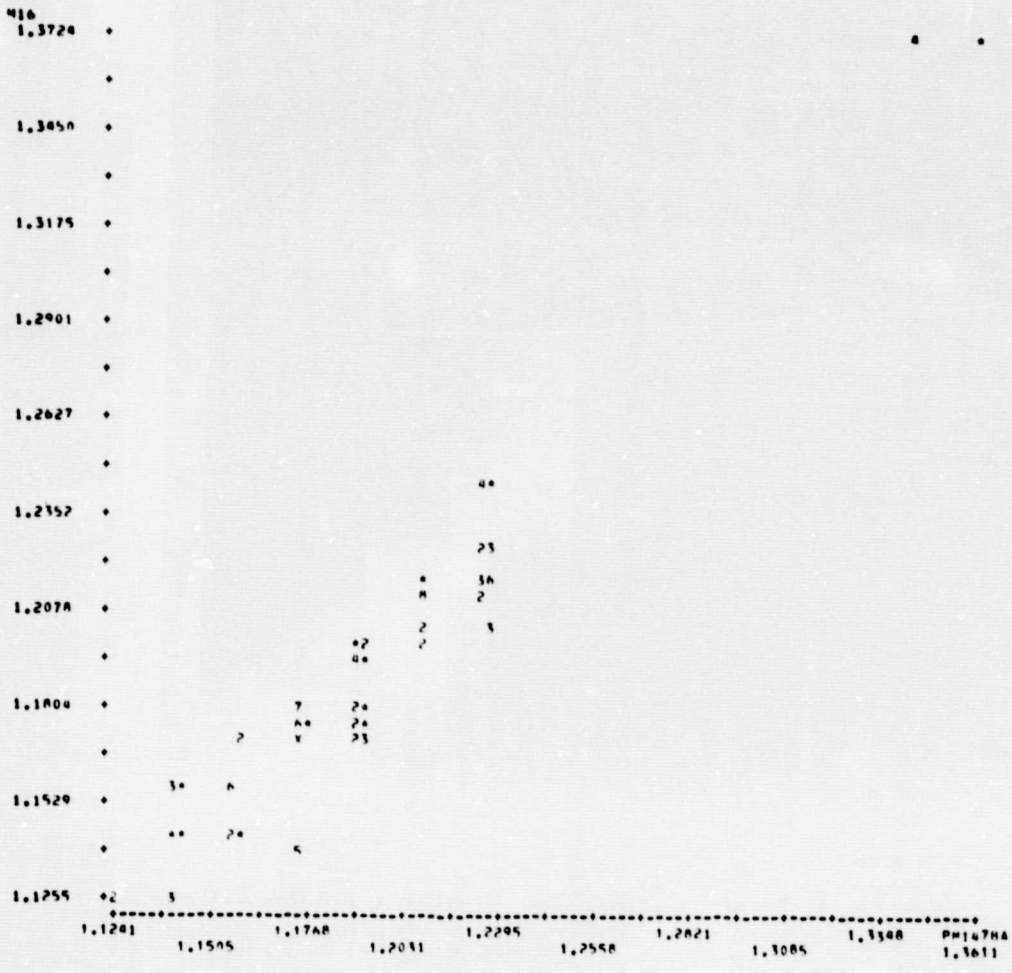

FIGURE 3. CORRELATION BETWEEN TRUE AND PREDICTED M_{16} VALUES (Vincent's Samples Only)

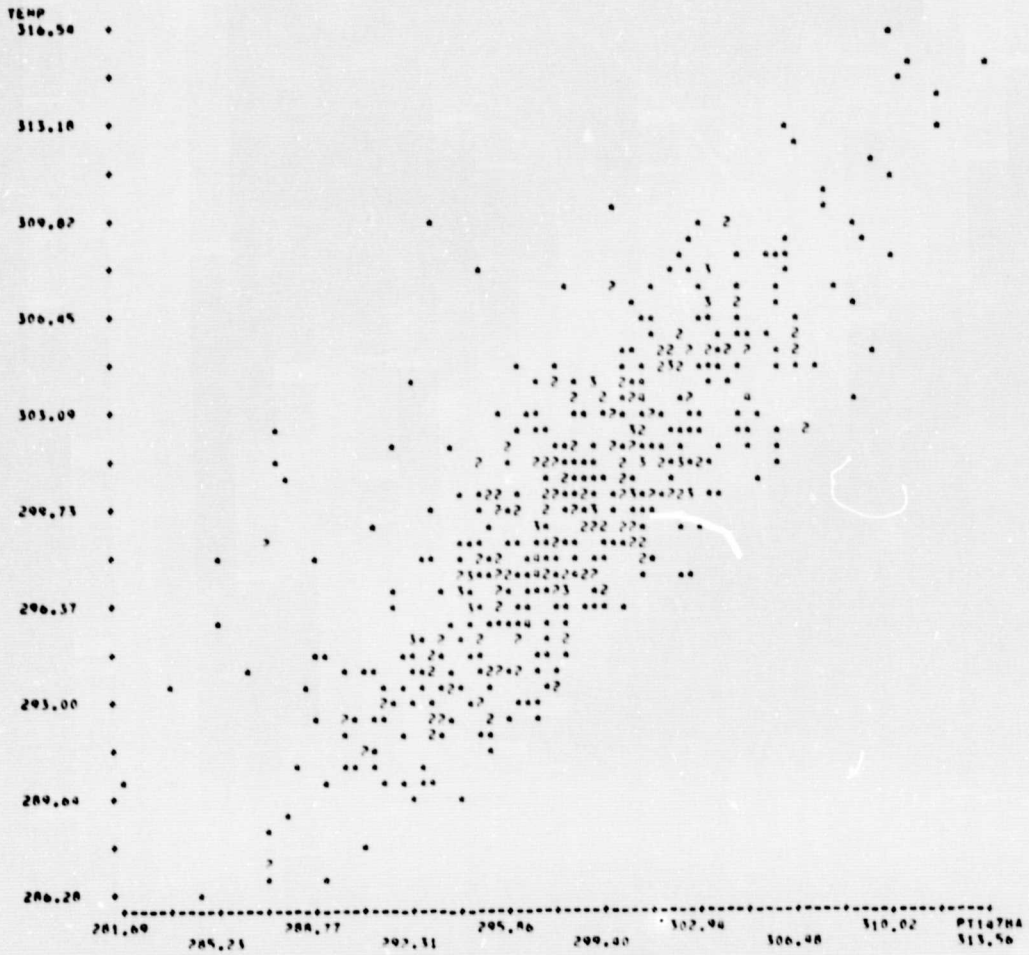

FIGURE 4. CORRELATION BETWEEN TRUE AND ESTIMATED VALUES OF TEMPERATURE (Hunt's Samples Only)

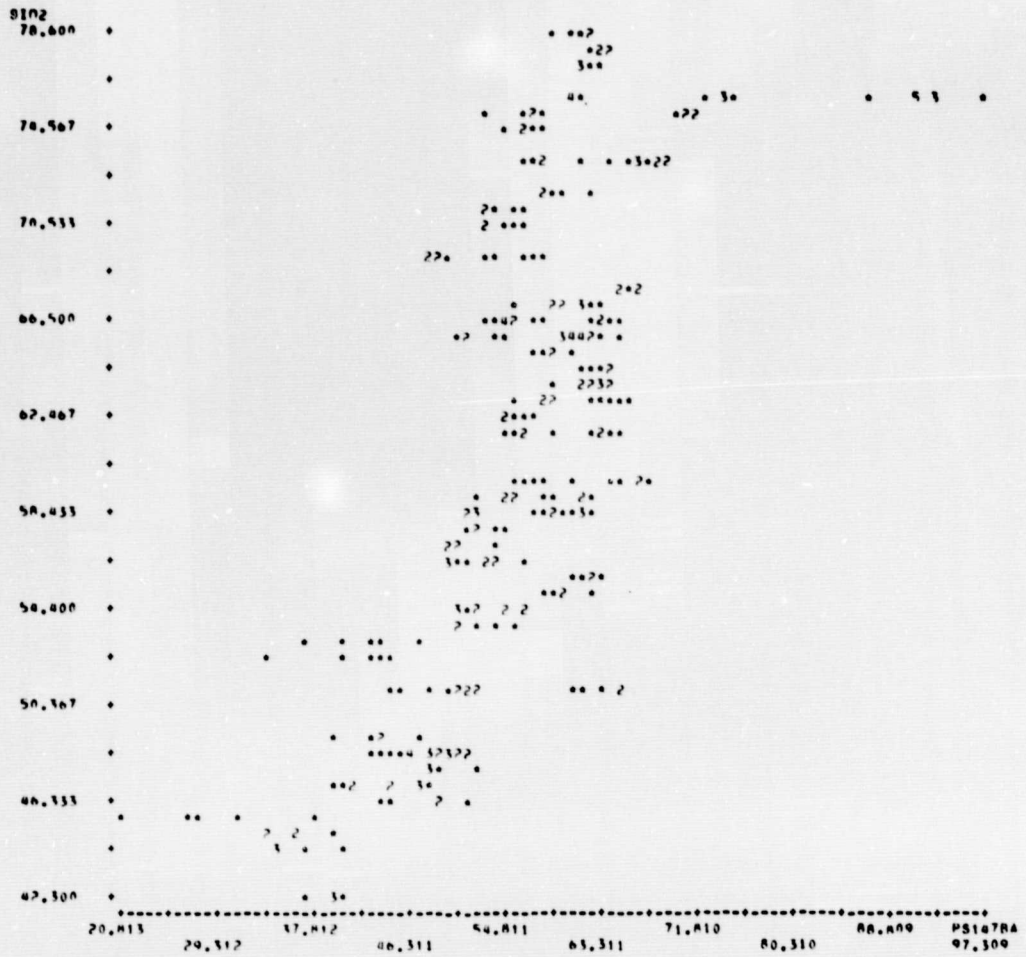

FIGURE 5. CORRELATION BETWEEN TRUE AND ESTIMATED VALUES OF % SiO_2
(Hunt's Samples Only)

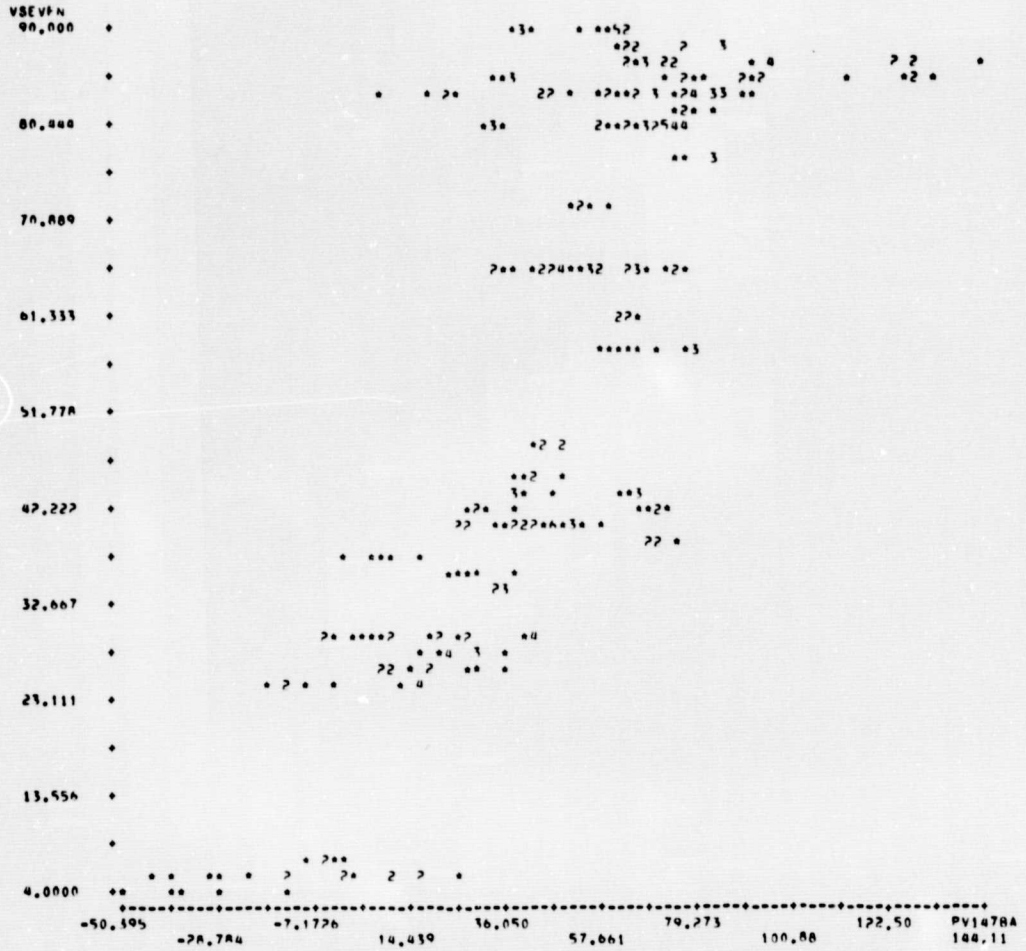

FIGURE 6. CORRELATION BETWEEN TRUE AND ESTIMATED VALUES OF V_7
(Hunt's Samples Only)

7
CONCLUSION

We emphasize that unfortunately the limited number of thermal infrared spectra available, as well as the small number of samples for which a quantitative mineral analysis had been performed, prevented a more detailed study in the field of general geologic mapping. Nevertheless, based on these simulations and analyses, the following conclusion was drawn: A thermal infrared imaging system with three 1 μm wide spectral bands located at 8.1-9.1 μm, 9.5-10.5 μm and 11.0-12.0 μm would provide an opportunity to estimate both sample temperatures and mineral parameters (% SiO_2, V_7 and M_{16}) from space.

APPENDIX

GROUPING OF IGNEOUS ROCK SPECTRA (Hunt, 1974)

		% SiO_2	V-7
1.	Aplite Granite 65	75.0	86
2.	Granite 70	69.0	85
3.	Graphic Granite 73	76.0	87
4.	Biotite Granite 76	67.0	85
5.	Hornblende Granite 150	75.9	85
6.	Granite 162	64.0	87
7.	Granite 245	72.9	89
8.	Granite 244	64.0	87
9.	Rhyolite 101	77.8	88
10.	Altered Rhyolite 55	68.1	90
11.	Rhyolite 98	78.6	90
12.	Tuff 87	74.6	90
13.	Green Lapilli Tuff 89	69.3	
14.	Lapilli Tuff 90	58.7	
15.	Tuff 61	71.1	
16.	Black Obsidian 52	77.0	
17.	Brown Obsidian 53	76.0	
18.	Pumice 62	70.8	
19.	Brown Obsidian 77	72.2	
20.	Vitrophyre 93	73.1	
21.	Perlite 72	75.0	
22.	Syenite 39	52.2	83
23.	Syenite 172	58.5	83
24.	Syenite 170	60.0	83
25.	Syenite 178	66.4	83
26.	"Nepheline" Syenite 83	59.1	81
27.	Trachyte 109	66.2	84
28.	Trachyte 42	55.3	82
29.	Trachyte 99	66.9	84
30.	Trachyte Porphyry 123	50.8	83
31.	Nepheline Syenite Porphyry 192	56.0	81
32.	Nepheline Syenite 100	59.3	81
33.	Nepheline Syenite 156	57.6	81
34.	Phonolite 157	48.0	81
35.	Phonolite 153	59.8	81
36.	Monzonite 233	53.8	66
37.	Monzonite Porphyry 234	62.8	66
38.	Quartz Monzonite 148	72.9	78
39.	Quartz Monzonite 149	61.8	73
40.	Monzonite 154	63.2	66
41.	Monzonite 173	65.4	66
42.	Latite 174	62.9	66
43.	Latite 175	57.3	66
44.	Biotite Granodiorite 235	65.8	62
45.	Granodiorite 64	61.8	58
46.	Dacite 56	65.8	58
47.	Tridymite Dacite 399		45
48.	Hornblende Diorite Porphyry 404		40
49.	Hornblende Diorite 152	48.7	38
50.	Diorite 403		40
51.	Hornblende Diorite 69	54.2	40
52.	Diorite Porphyry 44	56.1	42
53.	Hornblende Diorite 240	56.6	41
54.	Quartz Diorite 171	65.5	48
55.	Andesite 239	54.1	41
56.	Hornblende Andesite 236	65.9	39
57.	Andesite Porphyry 46	64.6	44
58.	Andesite 121	58.2	43
59.	Andesite 130	66.3	44
60.	Olivine Gabbro 158	44.2	24
61.	Hypersthene Gabbro 75	48.2	30
62.	Bytownite Gabbro 38	50.9	34
63.	Syenite Gabbro 159	51.3	36
64.	Hornblende Gabbro 132	45.2	30
65.	Diabase 129	48.2	28
66.	Diabase 131	52.9	30
67.	Diabase 238	46.9	27
68.	Diabase 242	46.1	27
69.	Diabase 155	48.1	29
70.	Olivine Basalt 166	46.7	25
71.	Flood Basalt 58	48.6	28
72.	Peridotite 410		5
73.	Peridotite 427		5
74.	Peridotite 118	42.3	7
75.	Peridotite 317		5
76.	Peridotite 128	45.8	4

GROUPING OF METAMORPHIC ROCK SPECTRA (Hunt, 1976)

77. Pink Marble 360B
78. Marble 457B
79. Dolomitic Marble 459B
80. Dolomitic Marble 458B
81. Serpentine Marble 460B
82. Red Quartzite 377B
83. Purple Quartzite 378B
84. Red Quartzite 379B
85. Gray Quartzite 382B
86. Green Quartzite 376B
87. Calcium Silicate Hornfels 471B
88. Hornfels 470B
89. Syenite Gneiss 467B
90. Albite Gneiss 390B
91. Felsic Gneiss 310B
92. Chloritic Gneiss 380B
93. Augen Gneiss 389B
94. Hornblende Gneiss 465B
95. Diorite Gneiss 464B
96. Sillimanite-Garnet Gneiss 466B
97. Slate 461B
98. Chiastolic Slate 462B
99. Gray Slate 307B
100. Phyllite 473B
101. Green Schist 392B
102. Tremolite Schist 469B
103. Hornblende Schist 241B
104. Tourmaline Schist 468B
105. Hornblende Schist 393B
106. Chlorite Schist 395B
107. Crumpled Mica Schist 394B
108. Graphite Schist 397

GROUPING OF IGNEOUS ROCK SPECTRA (Vincent, 1973)

		SiO_2	V-7	M_{16}
109.	Granite A79	76.7	80	1.1740
110.	Granite A119	66.2	68	1.1931
111.	Granite A122	72.4	76	
112.	Rhyolite SA-49	75.1	78	1.1255
113.	Rhyolite, Welded Tuff	76.1	79	1.1708
114.	Pyroxene Syenite E83A	61.4	82	1.1741
115.	Trachyte, Porphyritic	68.3	78	1.1578
116.	Nepheline Syenite	58.3	65	1.2094
117.	Granodiorite A117	53.6	43	1.2115
118.	Granodiorite A127	62.8	68	1.1691
119.	Dacite E12A	65.7	72	1.1726
120.	Dacite 2A1	66.9	60	1.1555
121.	Dacite 2B5	67.0	65	1.1412
122.	Diorite A129	61.0	54	1.1702
123.	Diorite E47C	56.2	40	1.1793
124.	Andesite E55A	57.8	45	1.1996
125.	Rhyolite 2A3	67.9	85	1.1423
126.	Gabbro E80A	50.6	24	1.1823
127.	Basalt 1A8	47.5	31	1.2146
128.	Basalt WI-1-104	48.0	30	1.2181
129.	Basalt S95	48.4	31	1.2271
130.	Basalt 5B4	48.3		
131.	Basalt 1A3	47.8	30	1.2033
132.	Anorthosite AN	49.7	19	1.2446
133.	Diabase	52.4	23	1.2188
134.	Peridotite EP-1	44.5	6	1.3724

REFERENCES

Anding, D., R. Kauth, R. Turner, 1970: Atmospheric Effects on Infrared Multispectral Sensing of Sea-Surface Temperature from Space, Willow Run Laboratories, WRL 2676-6-F, NAS12-2117.

Holmes, Q. A., D. R. Nuesch, 1978: Selection of a Seventh Spectral Band for the Landsat-D Thematic Mapper, ERIM Report 130100-4-F, NAS9-15362.

Hunt, G. R., R. K. Vincent, 1968: The Behavior of Spectral Features in the Infrared Emission from Particulate Surfaces of Various Grain Sizes, Journal of Geophysical Research, Vol. 73, No. 18, September 15, pp. 6039-6046.

Hunt, G. R., J. W. Salisbury, 1974: Mid-Infrared Spectral Behavior of Igneous Rocks, Air Force Cambridge Research Laboratories, Hanscom AFB, Massachusetts, AFCRL-TR-74-0625.

Hunt, G. R., J. W. Salisbury, 1975: Mid-Infrared Spectral Behavior of Sedimentary Rocks, Air Force Cambridge Research Laboratories, Hanscom AFB, Massachusetts, AFCRL-TR-75-0356.

Hunt, G. R., J. W. Salisbury, 1976: Mid-Infrared Spectral Behavior of Metamorphic Rocks, Air Force Cambridge Research Laboratories, Hanscom AFB, Massachusetts, AFCRL-TR-76-0003.

Kahle, A. B., 1977: A Simple Thermal Model of the Earth's Surface for Geologic Mapping by Remote Sensing, Journal of Geophysical Research, Vol. 82, No. 11, pp. 1673-1680.

Leeman, V., D. Earing, R. K. Vincent, S. Ladd, 1971: The NASA Earth Resources Spectral Information System: A Data Compilation, University of Michigan Technical Report 3165-24-T, NASA Contract NAS9-9784.

Lyon, R. J. P., 1964: Evaluation of Infrared Spectrophotometry for Compositional Analysis of Lunar and Planetary Soils, Rough and Powdered Surfaces, Final Report, Pt. 2, NASA Report CR-100.

Lyon, R. J. P., J. W. Patterson, 1969: Airborne Geological Mapping Using Infrared Emission Spectra, Proceedings of the Sixth International Symposium on Remote Sensing of Environment, University of Michigan, Ann Arbor, pp. 527-552.

Travis, R. B., 1955: Classification of Rocks, Quarterly of the Colorado School of Mines, Vol. 50, p. 12.

Vincent, R. K. and F. Thomson, 1971: Discrimination of Basic Silicate Rocks by Recognition Maps Processed from Aerial Infrared Data, Proceedings of the Seventh International Symposium on Remote Sensing of Environment, Ann Arbor, pp. 247-252.

Vincent, R. K. and F. Thomson, 1972a: Rock-Type Discrimination from Ratioed Infrared Scanner Images of Pisgah Crater, California, Science, Vol. 175, pp. 986-988.

Vincent, R. K. and F. Thomson, 1972b: Spectral Compositional Imaging of Silicate Rocks, Journal of Geophysical Research, Vol. 77, No. 14, pp. 2465-2471.

Vincent, R. K., 1973: A Thermal Infrared Ratio Imaging Method for Mapping Compositional Variations Among Silicate Rock Types, Ph.D. Dissertation, Dept. of Geology and Mineralogy, University of Michigan, Ann Arbor, Michigan.

Vincent, R. K., 1975: The Potential Role of Thermal Infrared Multispectral Scanners in Geological Remote Sensing, Proceedings of the IEEE, Vol. 63, pp. 137-147.

Watson, K., 1975: Geologic Applications of Thermal Infrared Images, Proceedings of the IEEE, Vol. 63, pp. 128-137.

Wheeler, S. G., P. N. Misra, and Q. A. Holmes, 1976: Linear Dimensionality of Landsat Data With Implications for Classification, Proceedings of Symposium on Machine Processing of Remotely Sensed Data, LARS, Purdue University, West Lafayette, Indiana.

Technical and Final Report Distribution List

NASA Contract NAS9-15362

NAME	NUMBER OF COPIES
NASA Headquarters **600 Independence Ave., S.W.** **Washington, D.C. 20546**	
Dr. I. Rasool/SS-1	(1)
Mr. Pitt Thome/ERB-2	(1)
Dr. James Morrison/ERD-2	(1)
Dr. Murray Felsher/ER-1	(1)
Ms. Ruth Whitman/ERD-2	(1)
Mr. Mike Calabrese/ERB-2	(1)
NASA/Goddard Space Flight Center **Greenbelt, Maryland 20771**	
Dr. Vincent V. Salomonson/Code 913 (Landsat D Project Scientist)	(3)
Dr. Louis S. Walter/Code 920	(1)
Dr. A. Rango/Code 913	(1)
Mr. Charles R. Gunn/Code 400.8 (Landsat D Project Manager)	(1)
Dr. Charles Schnetzler/Code 923.0	(1)
Mr. Kenneth I. Duck/Code 720.2	(1)
Dr. Stanley C. Freden/Code 902	(1)
Dr. John L. Barker/Code 923.0	(1)
Dr. Compton J. Tucker/Code 923.0	(1)
Dr. Paul D. Lowman/Code 922.0	(1)
Dr. Nicholas M. Short/Code 923.0	(1)
Mr. Herbert W. Blodget/Code 923.0	(1)
Mr. Oscar Weinstein/Code 726.0	(1)

NAME	NUMBER OF COPIES
NASA/Jet Propulsion Laboratory 4800 Oak Grove Dr. Pasadena, California 91103	
Dr. Alexander F. H. Goetz/Code 183-501	(1)
Dr. Anne B. Kahle/Code 183-501	(1)
NASA/Johnson Space Center Houston, Texas 77058	
Mr. Gene T. Rice/HA	(1)
Mr. Olav Smistadt/HB	(1)
Mr. Richard A. Moke/HC	(1)
Mr. M. Jay Harnage, Jr./HC	(1)
Mr. Gerald P. Kenney/HC	(1)
Mr. Harold E. Granger/HD	(1)
Mr. Robert K. Stewart/HD	(10)
Dr. Robert B. MacDonald/SF	(1)
Dr. Forrest G. Hall/SF	(1)
Dr. Jon D. Erickson/SF3	(1)
Mr. Mickey C. Trichel/SF3	(1)
Mr. William E. Hensley/SF4	(1)
Dr. Phil Weber/SF5	(1)
Mr. Allen L. Grandfield/SF3	(1)
Dr. Richard P. Heydorn/SF3	(1)
Mr. Theodore K. Sampsel/ED6	(1)
Mr. Rex R. Ritz/BB6	(1)
Mr. Ben T. McGuire/BB6	(1)
Ms. Retha Shirkey/JM6	(1)
Mr. Eugene L. Davis, Jr./FM	(1)

NAME	NUMBER OF COPIES
U.S. Geological Survey Federal Center Denver, Colorado 80225	
Dr. Graham R. Hunt	(1)
Dr. J. Taranik	(1)
Mr. H. Curfman, Code 422 NASA/Langley Research Center Hampton, Virginia 23665	(1)
Dr. Fred B. Henderson, III The Geosat Committee 690 Market Street Suite 1400 San Francisco, California 94104	(5)
Mr. Samuel C. Coroniti Office of the Secretary of Transportation Washington, D.C. 20590	(1)
Mr. John Kousandreas Waterside Mall Room 3809 41 M Street, S.W. Environmental Protection Agency Washington, D.C. 20460	(1)
Dr. Gordon Law Assistant and Science Advisor to the Secretary U.S. Department of Interior Washington, D.C. 20242	(1)
Mr. L. P. Murphy ETL-GS-P U.S. Army Engineer Topographic Laboratories Department of the Army Fort Belvoir, Virginia 22050	(1)

NAME	NUMBER OF COPIES
Dr. Charles K. Paul Manager, Remote Sensing Programs Agency for International Development Department of State Washington, D.C. 20523	(1)
Mr. Robin Rowley/HD NASA/Johnson Space Center Houston, Texas 77058	(1)
Mr. Jack W. Sherman, III Chief, Spacecraft Oceanography Group National Environmental Satellite Service National Oceanic and Atmospheric Administration Washington, D.C. 20233	(1)
Dr. George E. Winzer Chief of the Environment and Land Use and Research Group Housing and Urban Development Washington, D.C. 20410	(1)
Mr. George Robcheosky Rainbow Systems 206 N. Washington Street Alexandria, Virginia 22314	(2)
Dr. Clifford Harlan Texas A&M University Remote Sensing Center College Station, Texas 77843	(1)
Dr. Craig Wiegand U.S. Department of Agriculture Soil & Water Conservation Research Division P.O. Box 267 Weslaco, Texas 78596	(1)

NAME	NUMBER OF COPIES
Goddard Institute of Space Studies Columbia University New York City, New York 10025	
Dr. Stephen G. Ungar	(1)
Ms. Vivien Gornitz	(1)
LARS/Purdue University Purdue Industrial Research Park 1200 Potter Drive West Lafayette, Indiana 47906	
Dr. David Landgrebe	(1)
Dr. Marvin E. Bauer	(1)
Dr. Roger Hoffer	(1)
U.S. Geological Survey 1925 Newton Square E. Reston, Virginia 22090	
Dr. Alden P. Colvocoresses	(1)
Dr. John Denoyer Director, EROS Program Bldg. E2	(1)
Dr. Larry Rowan, Mail Stop 927	(1)
Dr. Melvin M. Podwysocki	(1)
Dr. William E. Fischer	(1)
Mr. Stephen J. Gawarecki	(1)
Mr. W. Douglas Carter	(1)
Mr. Moe Deutsch	(1)

NAME	NUMBER OF COPIES
Dr. Robert K. Vincent Geospectra Corporation 320 N. Main Street Suite 301 Ann Arbor, Michigan 48104	(2)
Dr. Floyd Sabins Chevron Oil Field Research Company Standard Oil Company of California, Subsidiary P.O. Box 446 La Habra, California 90631	(1)
Dr. William L. Smith Spectral Data 8100 Cawdorn Port McLean, Virginia 22101	(1)
Dr. Ronald J. P. Lyon Stanford University Palo Alto, California 94305	(1)
Dr. Farouk El Baz Research Director National Air & Space Museum Room 3101 Washington, D.C. 20560	(1)
Mr. Winfred E. Berg National Research Council Committee on Remote Sensing Programs for Earth Resource Surveys 2101 Constitution Avenue Washington, D.C. 20418	(3)
Dr. John W. Salisbury Department of Energy 20 Massachusetts Avenue, N.W. Mail Stop 3122C Washington, D.C. 20545	(1)